Supplementary Information

Creation of Immiscible OsPd Solid Solution as Rh-free Catalyst with NO_x Reduction Performance Overpassing Rh

Bo Huang,*[a,b,c] Ying Qin,[a,b] Junyun Gao,[a,b] Zhe Tan*[b,c] and Hong Zheng*[d]

[a]School of Chemical Engineering and Technology, Xi'an Jiaotong University, Innovation Harbour, Xixian-ward, Xi'an 712000, China.

[b]Shaanxi Tianyi Element Technology Co., Ltd, High-tech industrial development zone, Xianyang 712000, China.

[c]National Innovation Platform (Center) for Industry-Education Integration of Energy Storage Technology, Xi'an Jiaotong University. Innovation Harbour, Xixian-ward, Xi'an 712000, China.

[d]The Key Laboratory of Electrical Insulation and Power Equipment, Center of Nanomaterials for Renewable Energy, School of Electrical Engineering, Xi'an Jiaotong University, Xi'an 710049, China.

E-mail: B.H. (bohuang@xjtu.edu.cn), Z.T. (tanzhe@stu.xjtu.edu.cn), H.Z. (zhenghong666@xjtu.edu.cn)

Materials and Methods

Synthesis of Rh nanoparticles. To synthesize Rh NPs, an ethylene glycol solution (EG, 20 ml) containing $Na_3RhCl_6 \cdot 12H_2O$ (300.4 mg, 0.5 mmol) was added into a mixture solution of PVP (110 mg, 1 mmol) and diethylene glycol (DEG, 80 ml) at 220 °C under ambient condition with magnetic stirring. The reaction was kept for 15 min and cooled to room temperature. The black powder was collected by same post-treatment as OsPd NPs.

Synthesis of Rh/γ-Al_2O_3 *via* impregnation method. γ-Al_2O_3 (1018.7mg, precalcined at 873 K for 5 h) was added into 10 ml water containing $RhCl_3 \cdot xH_2O$ (22.7mg, 0.1 mmol) and stirred for 4 h. The solution was dried overnight at 110 °C in an oven, and then calcined at 600 °C for 3 h. Before testing its NO_x reduction performance, the catalyst was reduced with 10% H_2/Ar (20 ml·min^{-1}) at 300 °C for 30 min.

Synthesis of Os/γ-Al_2O_3 catalyst. To synthesize Os/γ-Al_2O_3 catalyst, an triethylene glycol (TEG, 15 ml) and DEG (5 ml) mixture solution containing $K_2OsCl_6 \cdot 12H_2O$ (962.0 mg, 2 mmol) was added into a mixture solution of PVP (440 mg, 4 mmol) and TEG (150 ml) at 240 °C under ambient condition with magnetic stirring. The reaction was kept for 10 min and cooled to room temperature. The black powder of Os NPs was collected by same post-treatment as OsPd NPs. The method for Os NPs supported on γ-Al_2O_3 as Os/γ-Al_2O_3 catalyst was described in detail in catalyst preparation section.

Synthesis of Pd/γ-Al_2O_3 catalyst. To synthesize Pd/γ-Al_2O_3, an EG solution (30 ml) containing K_2PdCl_4 (652.8 mg, 2 mmol) was added into a mixture solution of PVP (440 mg, 4 mmol) and DEG (130 ml) at 220 °C under ambient condition with magnetic stirring. The reaction was kept for 15 min and cooled to room temperature. The black powder was collected by same post-treatment as OsPd NPs. The method for Pd NPs supported on γ-Al_2O_3 as Pd/γ-Al_2O_3 catalyst was described in detail in catalyst preparation section.

Characterizations. The crystal structures were investigated by XRPD analysis using a Bruker D8 Advance diffractometer (Cu $K\alpha$ radiation). The atomic ratios of Os and Pd in the alloys were investigated by XRF and EDX spectroscopies using Bruker S8 Tiger and Talos F200X, respectively. HAADF-STEM and STEM-EDX mapping analyses were recorded on Talos F200X operated at 200 kV accelerating voltage.

Catalyst preparation. The synthesized OsPd and Rh NPs were supported on γ-Al_2O_3 catalysts by wet impregnation. Each NP (equivalent to 1 wt% of γ-Al_2O_3) was dispersed by ultrasonication in purified water. The γ-Al_2O_3 support has been precalcined at 873 K for 5 h. The precalcined γ-Al_2O_3 was added into each NP solution, and then the suspended solutions were stirred for 12 h. After stirring, the suspended solutions were heated to 60 °C and dried under vacuum. The resulting powders were kept at 120 °C for 8 h for complete water removal. The loading amounts of metals were confirmed by XRF measurements.

NO_x reduction activity measurements. Before investigation of catalytic activity, each supported NP catalyst was pre-treated under reducing atmosphere to remove surface oxidized layer. The OsPd and Rh NPs on γ-Al_2O_3 catalysts were heated under 200 °C with 5% H_2/Ar gas flow (20 ml·min^{-1}) for 30 min. For the investigation of catalytic activity in NO_x reduction, each pre-treated catalyst (50 mg) was loaded into a tubular quartz reactor (internal diameter, i.d. 7 mm) with quartz wool. A gas mixture of 1% NO / 2% CO / Ar with flow rate of 15 / 15 / 200 sccm) was passed over the catalysts at ambient temperature. After 15 min, effluent gas was collected, and the reaction products were analysed by NO_x analyser (SV-5Q, Tianjin Shengwei Development of Science Co., Ltd.). The catalysts were heated up to 460 °C, and the products were analysed at each temperature after 10 min to reach the equilibrium condition. After the reaction, the reactor was purged with Ar at the reaction temperature, and the catalysts were then cooled to room temperature.

***In situ* Fourier transform infrared (FTIR) measurements.** Each sample was loaded into a crucible and placed in an infrared cell. Pretreated the samples at 200 °C under 5% H_2/Ar flow for 10 min, then cooled down to 50 °C. For *in situ* FTIR

measurements under CO flow, the activated samples were exposed to 2% CO/Ar flow at 50 °C for 10 min. Then raised the temperature to 200 °C directly at a rate of 10 °C/min. For *in situ* FTIR measurements under NO + CO flow, the above sample was exposed to 1% NO/Ar + 2% CO/Ar flow at 200 °C for 10 min, then to only 1% NO/Ar flow for 20 min at last. IR spectra were recorded at the interval of 30 seconds using a Nicolet iS50 FTIR spectrometer, accumulating 49 scans at a resolution of 4 cm^{-1}.

DFT calculation. Before the construction of solid solution model of OsPd alloy, we firstly constructed a Rh crystal of fcc lattice. This Rh crystal was optimized with the Perdew-Burke-Ernzerhof (PBE) exchange functional[1] and the D3 method of Grimme[2] was employed. The projector augmented wave (PAW) method was employed to describe the interactions between valence shells and the ionic core. The kinetic energy cutoff was set as 400 eV and a k-mesh of 8×8×8 was adopted. Then, we constructed a solid solution model of OsPd alloy based on a 2×2×2 supercell of Rh crystal, in which 16 Os atoms and 16 Pd atoms were mixed randomly. After optimization of this OsPd alloy, the (111) surface of it was constructed, in which a vacuum space of 20 Å was employed to avoid interaction between the surfaces. 4 atomic layers were included in the surface models. In the optimization of this surface model, the bottom 2 atomic layers were fixed and the k-mesh was set as 3×3×1.

In the investigation of NO cleavage, different adsorption sites of NO molecule were calculated with the same computational parameters as the optimization of OsPd surface. It was found that NO prefers to be adsorbed by an Os atom to form O-N··· Os. The final structure after NO cleavage was also optimized, in which the O atom is adsorbed by a Pd atom. Then, the climbing-image nudged elastic band (CI-NEB) method was used to describe the cleavage process of NO, in which five points were included between pristine adsorption model and final cleavage model. The Gibbs free energy (G) of each structure was evaluated as follows:

$$\Delta G = \Delta E + \Delta E_{ZPE} + T\Delta S \quad (1)$$

Where ΔE term is the reaction energy obtained by DFT calculations. ΔE_{ZPE} and $T\Delta S$ are the zero-point energy correction and entropy change, respectively. Note that T is the experimental temperature at 473 K.

For comparison, the (111) surface of the Rh crystal was also constructed and NO cleavage on Rh surface was investigated with the same method as above.

For the investigations of CO adsorption, we calculated an adsorption model on the (111) surface of the OsPd alloy, where the CO molecule was adsorbed on top site of an Os atom in the form of O-C···Os. For comparison, adsorption of CO on the surface of Os crystal was also calculated. An fcc Os crystal was firstly constructed and its (111) surface model, including 4 atomic layers and 32 Os atoms, was optimized. Then, the adsorption of CO on the Os surface in the form of O-C···Os was calculated. The computational parameters of structural optimization and vibrational frequency of adsorbate (used for calculation of free energy and analysis of infrared spectra) were the same as the calculations of NO adsorption.

All the DFT calculations were carried out with the Vienna *ab initio* Simulation Package (VASP).[3]

Characterization Data

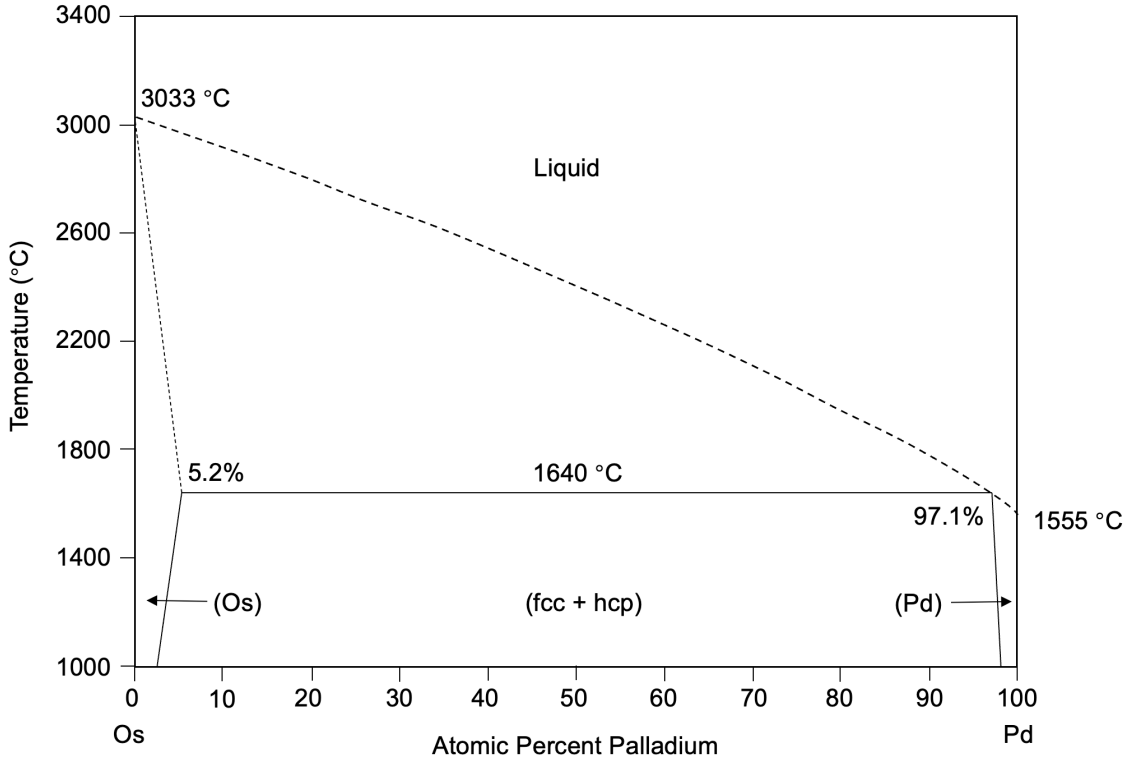

Figure S1. Os-Pd phase diagram redrawn from reference: M.A. Tylkina, V.P. Polyakova, and O.Kh. Khamidov, *Zh. Neorg. Khim.*, 1963, 8, 776-778, in Russian; TR: *Russ. J. Inorg. Chem.*, 1963, 8, 395-397.

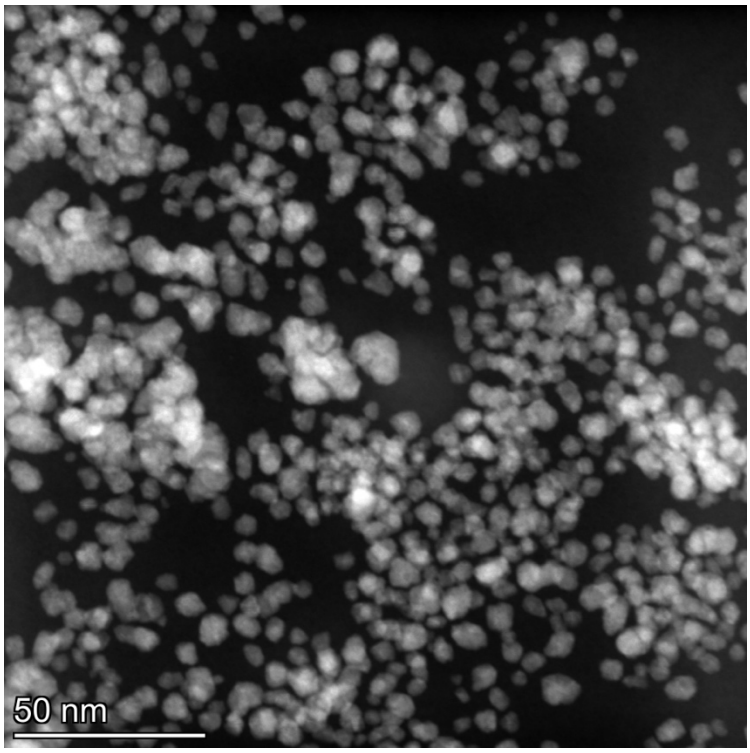

Figure S2. HAADF-STEM image of OsPd NPs.

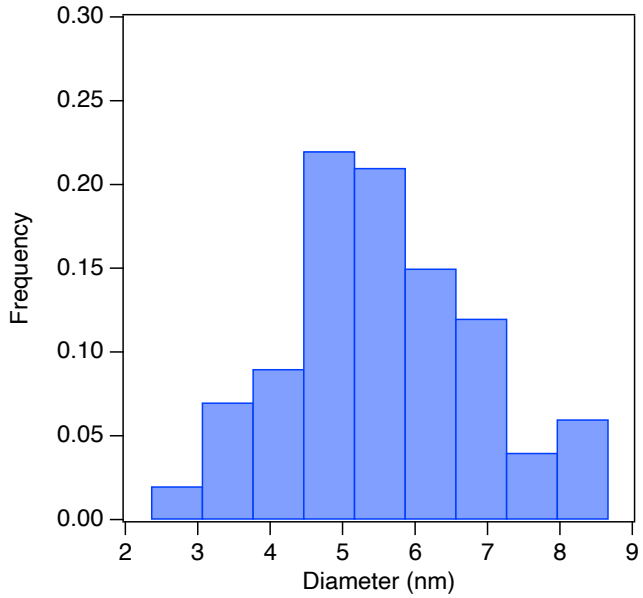

Figure S3. Size distribution of OsPd NPs. The mean diameter of OsPd NPs is 5.3 ± 1.1 nm.

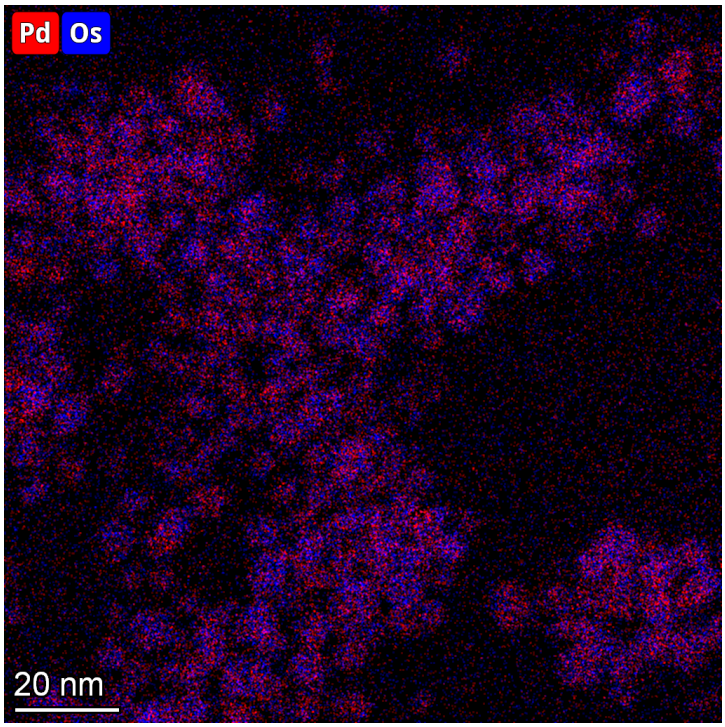

Figure S4. HAADF-STEM EDX mapping image of OsPd NPs. The Os : Pd ratio in this area was 0.53 : 0.47.

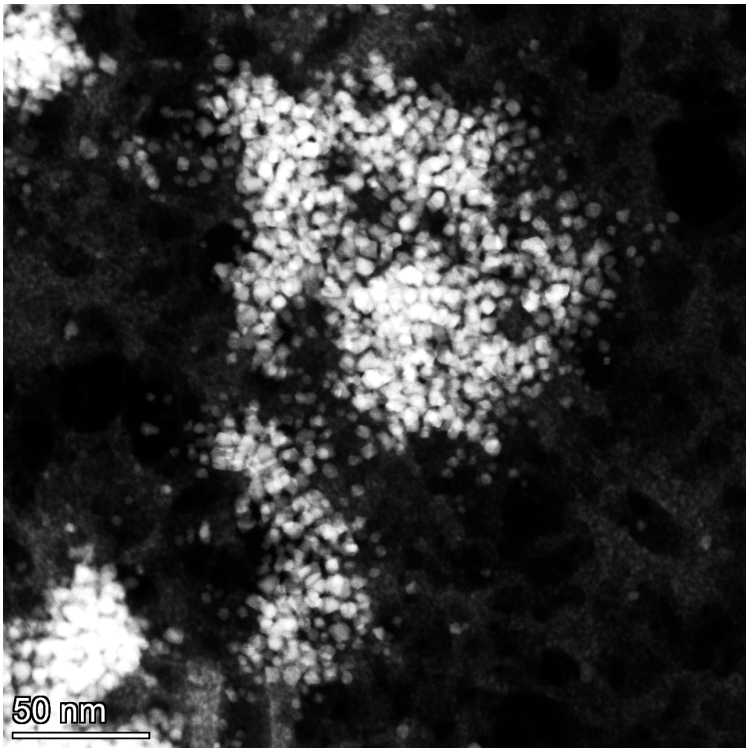

Figure S5. HAADF-STEM image of Rh NPs.

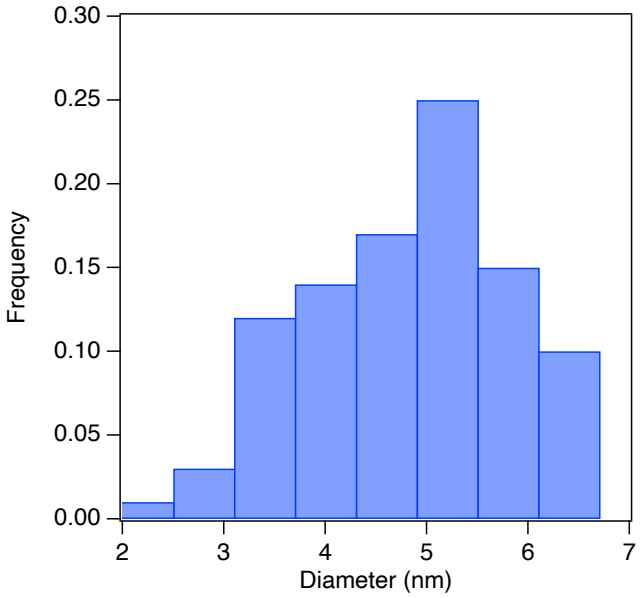

Figure S6. Size distribution of Rh NPs. The mean diameter of Rh NPs is 4.6 ± 0.9 nm.

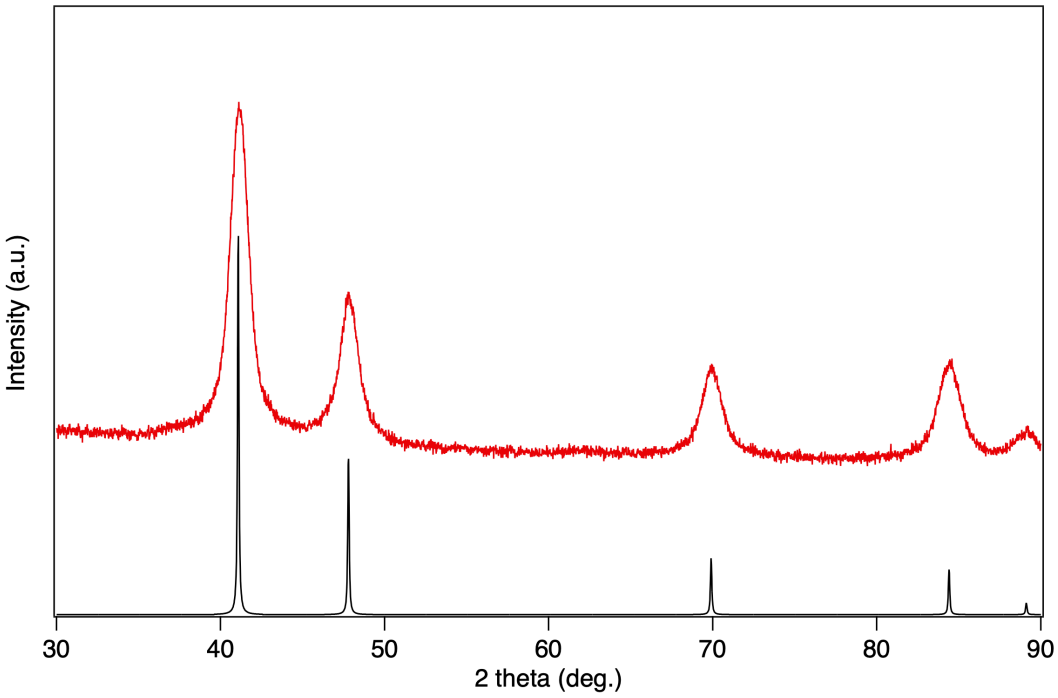

Figure S7. XRPD patterns of Rh NPs (red) and the simulated Rh bulk (black) at 303 K. The radiation wavelength was 1.54056 Å.

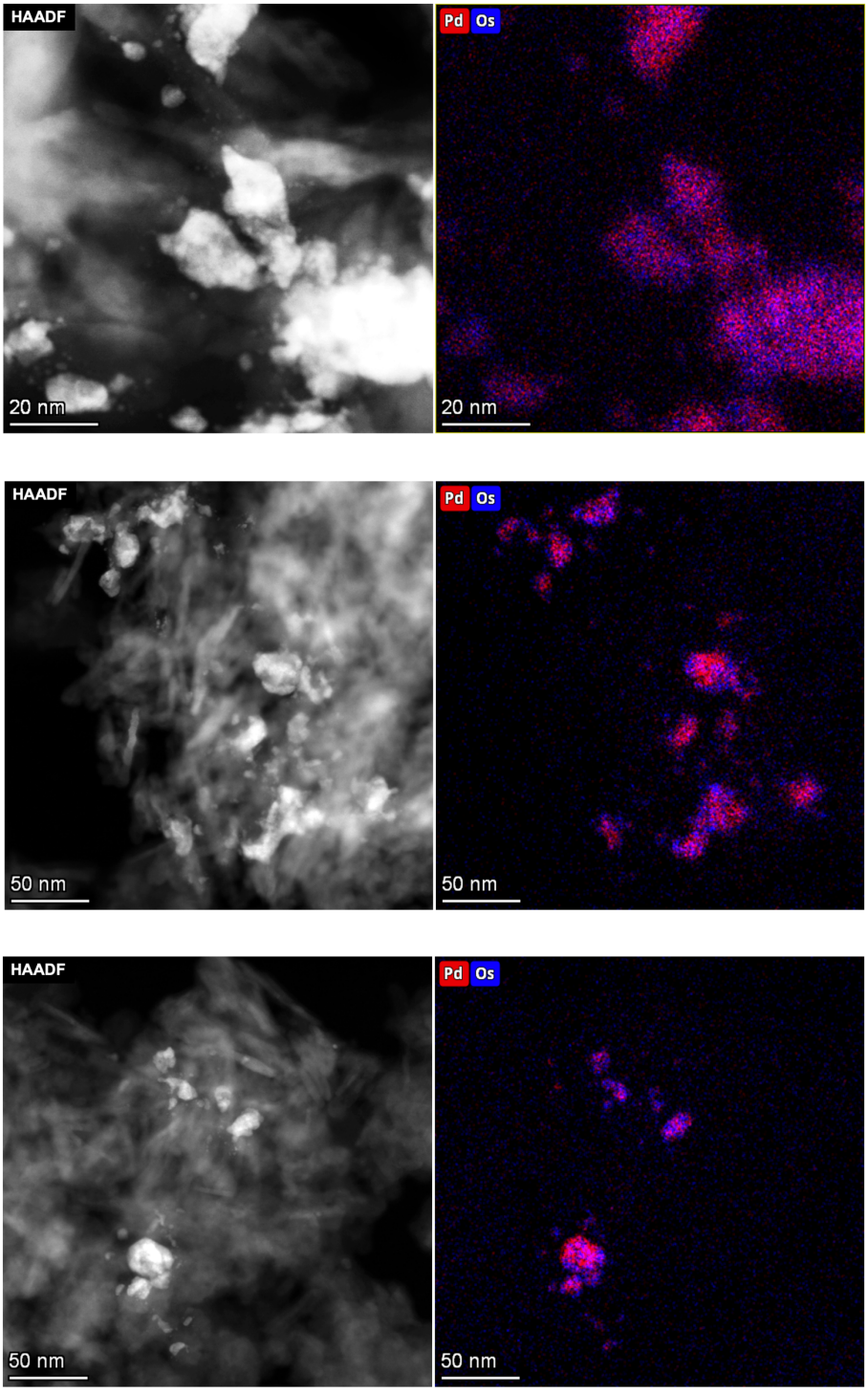

Figure S8. HAADF images and reconstructed overlay images of Os-L STEM-EDX maps and Pd-L STEM-EDX maps obtained from groups of OsPd NPs after reaction (red, Pd; blue, Os).

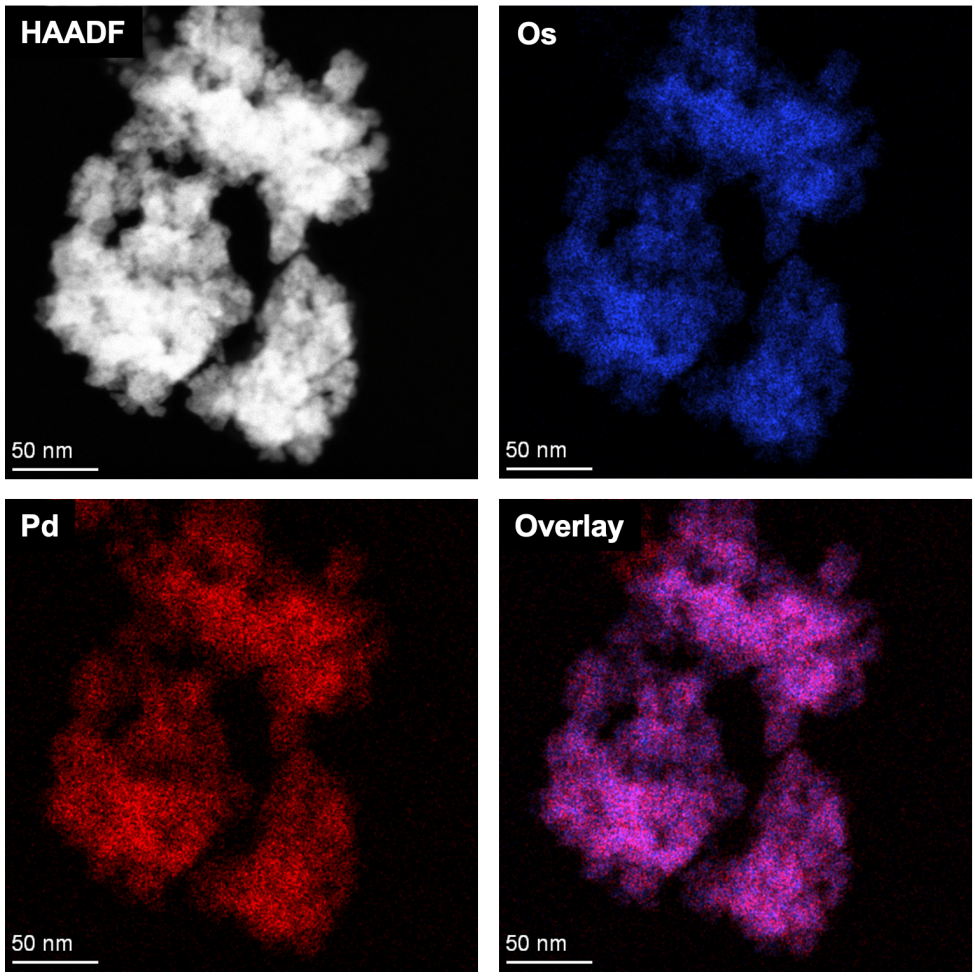

Figure S9. HAADF-STEM image, Os-L STEM-EDX map (blue), Pd-L STEM-EDX map (red), and an overlay map of Os and Pd distributed in the OsPd solid solution annealed at 750 °C under Ar atmosphere for 1 h.

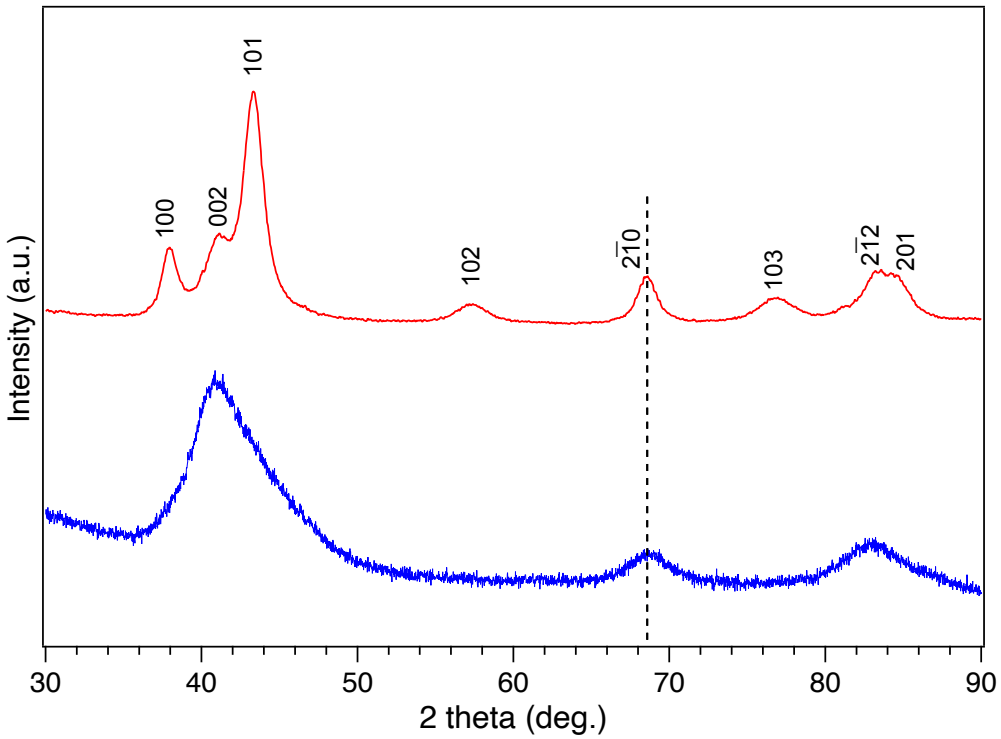

Figure S10. XRPD patterns of as-synthesized OsPd solid solution (blue) and the OsPd solid solution (red) annealed at 750 °C under Ar atmosphere for 1 h. The radiation wavelength was 1.54056 Å. The dashed line shows the peak position of {$2\bar{1}0$} diffraction planes of hcp-structured OsPd solid solution.

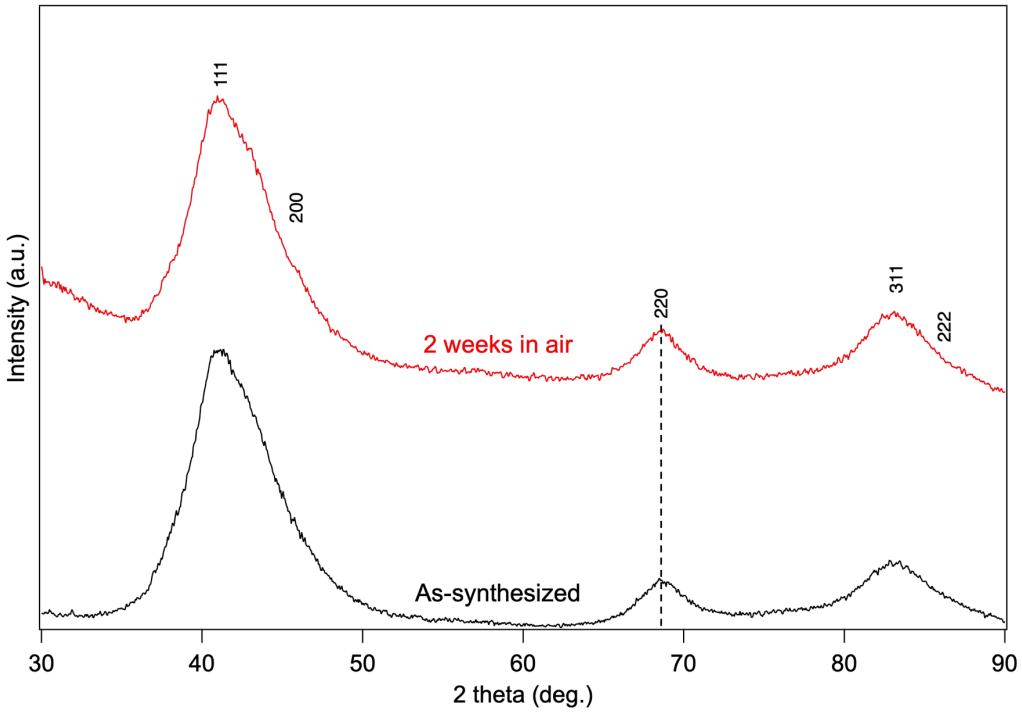

Figure S11. XRPD patterns of as-synthesized OsPd solid solution (black) and the OsPd solid solution (red) kept in air for 2 weeks. The radiation wavelength was 1.54056 Å. The dashed line shows the peak position of {220} diffraction planes of OsPd solid solution.

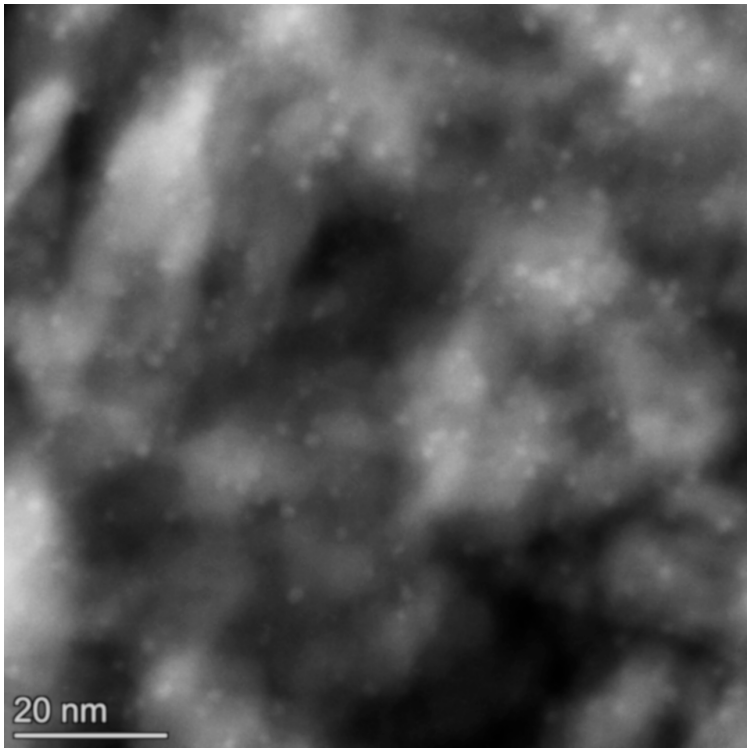

Figure S12. HAADF-STEM image of Rh/γ-Al_2O_3 catalyst prepared by impregnation method.

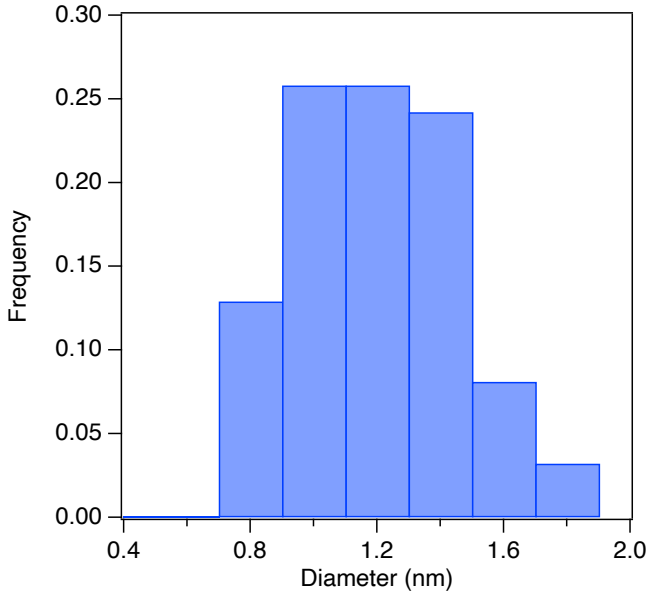

Figure S13. Rh NP size distribution in Rh/γ-Al_2O_3 catalyst prepared by impregnation method. The mean diameter of Rh NPs is 1.2 ± 0.3 nm.

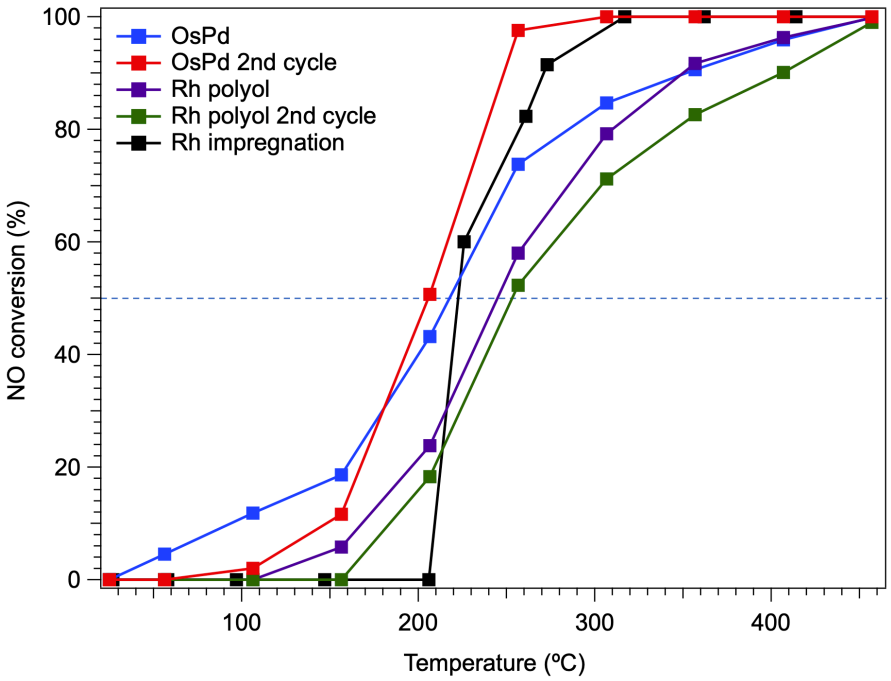

Figure S14. NO conversion in NO_x reduction reaction for OsPd solid solution, pure Rh NPs prepared by polyol method and impregnation method on γ-Al_2O_3. The dashed line shows the 50% conversion.

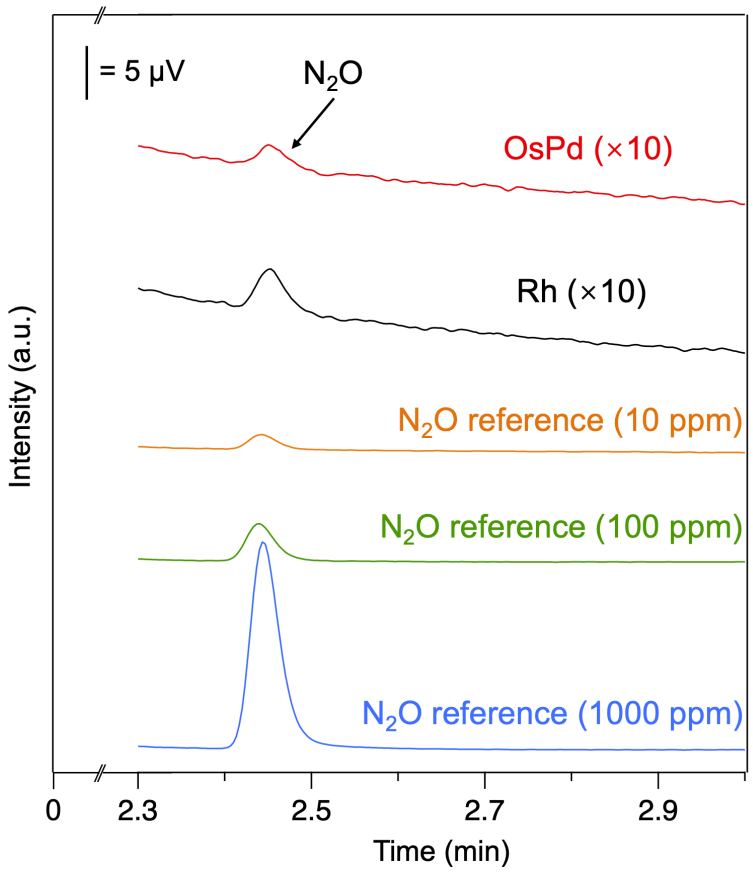

Figure S15. Gas-chromatography spectra for reaction gases from OsPd and Rh catalysts collected at 200 °C. Other conditions were fixed same with the NO_x reduction reaction. The N_2O references were prepared by mixing different volumes of pure N_2O with air.

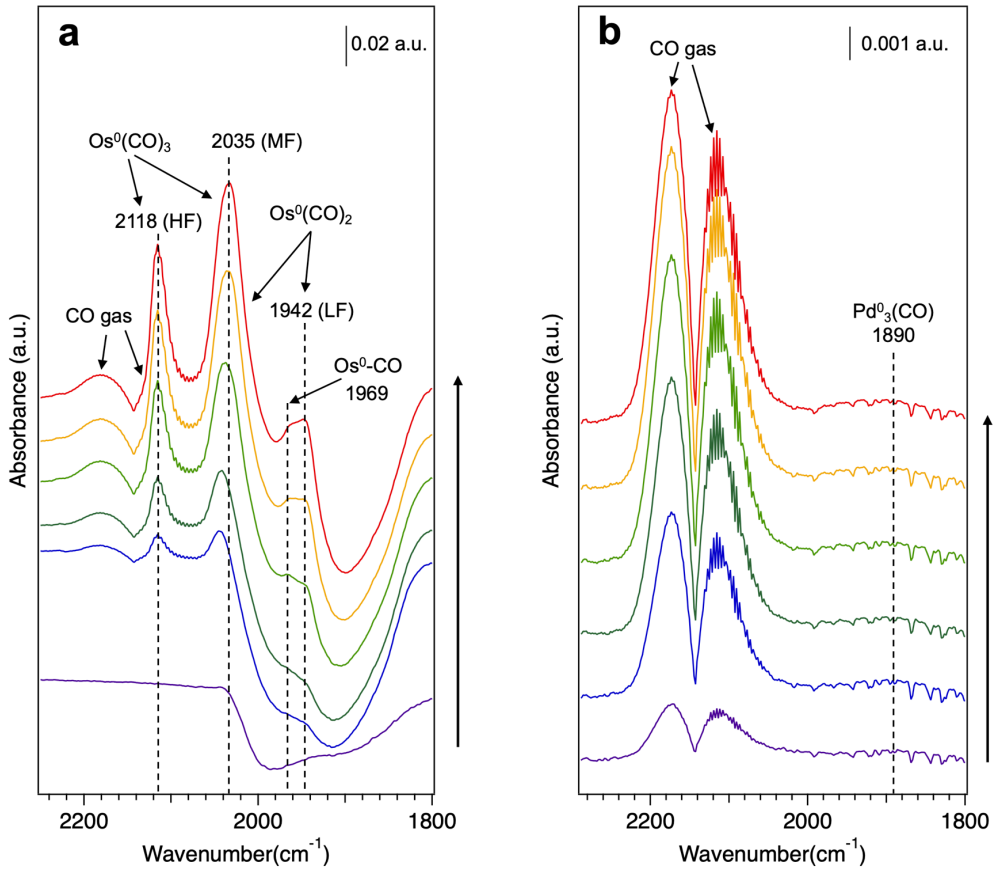

Figure S16. *In situ* FTIR measurements on (a) Os catalyst under CO flow at 200 °C and (b) Pd catalyst under CO flow at 50 °C. All intervals between these spectra are 1 min. HF, MF and LF stand for higher-frequency, medium-frequency and lower-frequency bands, respectively.

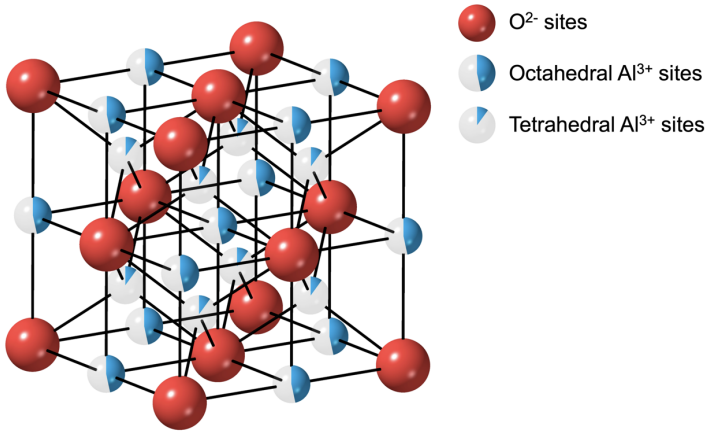

Figure S17. The crystal structure of γ-Al_2O_3. Octahedral and tetrahedral Al^{3+} sites are shown with their occupancy by pie chart on Al^{3+} ions, with 0.466 and 0.1 for octahedral and tetrahedral sites, respectively. The crystal information file is from literature of E. J. W. Verwey, *Zeitschrift fur Kristallographie* 1935, 91, 317.

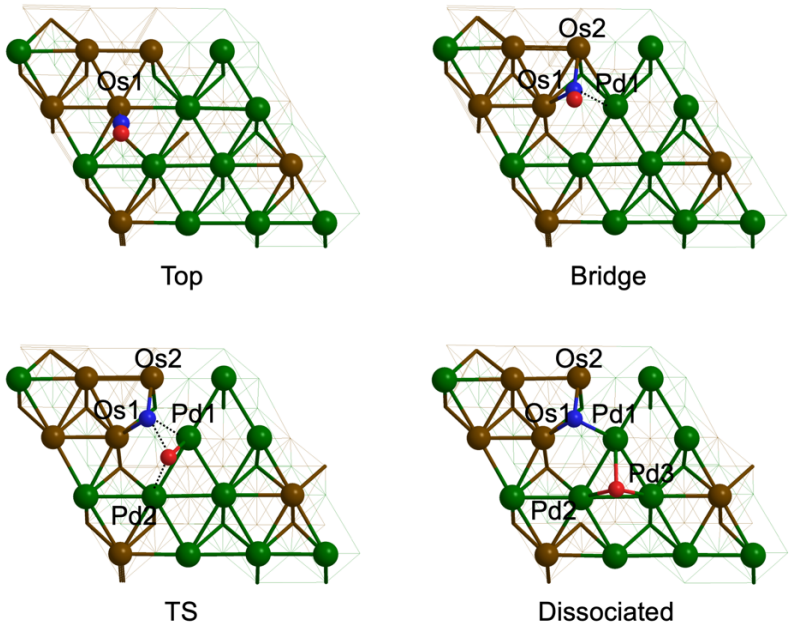

Figure S18. The adsorption sites of NO dissociation on (111) facet of OsPd solid solution.

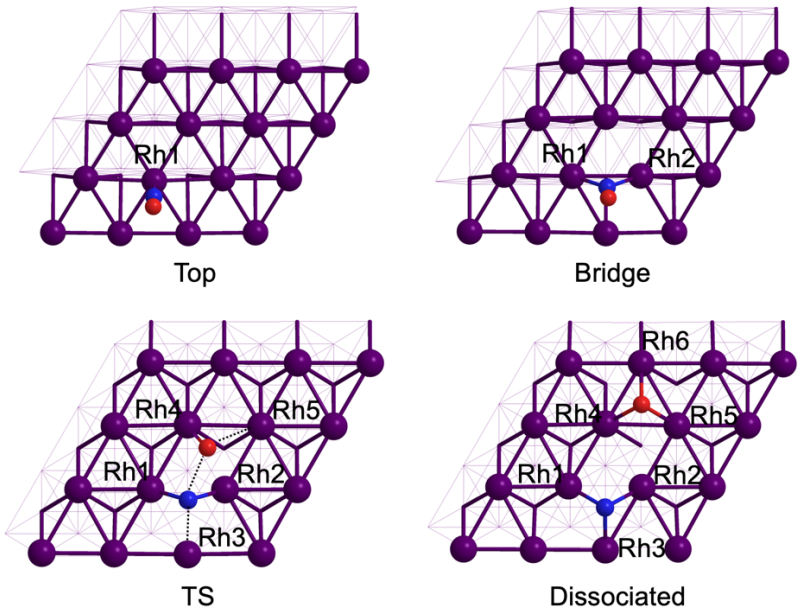

Figure S19. The adsorption sites of NO dissociation on (111) facet of Rh.

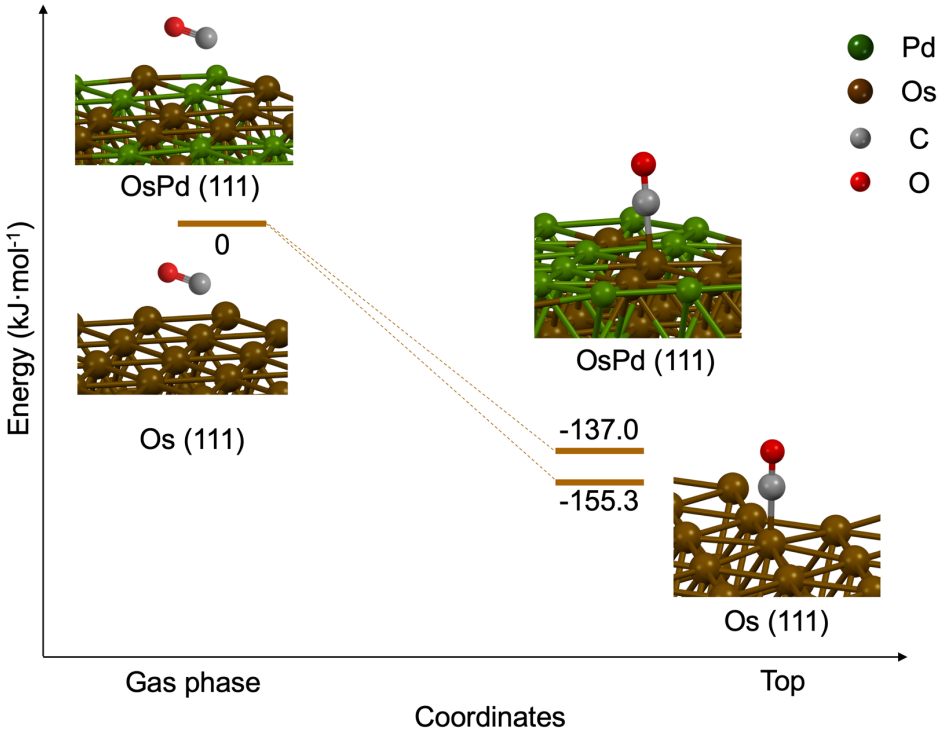

Figure S20. DFT calculations for CO adsorption processes on OsPd (111) and Os (111) surfaces.

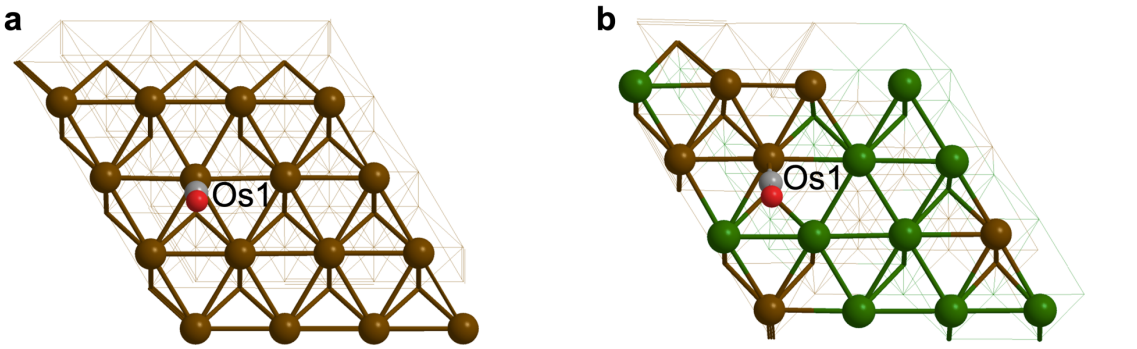

Figure S21. The CO adsorption sites on (111) facet of (a) Os and (b) OsPd.

References

1. A. V. Krukau, O. A. Vydrov, A. F. Izmaylov, G. E. Scuseria, Influence of the exchange screening parameter on the performance of screened hybrid functionals. *J. Chem. Phys.*, **125**, 224106 (2006).
2. S. Grimme, J. Antony, S. Ehrlich, H. Krieg, A consistent and accurate ab initio parametrization of density functional dispersion correction (DFT-D) for the 94 elements H-Pu. *J. Chem. Phys.*, **132**, 154104 (2010).
3. G. Kresse, J. Furthmüller, Efficient iterative schemes for ab initio total-energy calculations using a plane-wave basis set. Phys. Rev. B: Condens. *Matter Mater. Phys.*, **54**, 11169 (1996).